# Structure and properties of silica nanoclusters at high temperatures

I. V. Schweigert,* K. E. J. Lehtinen,[†] M. J. Carrier,[‡] and M. R. Zachariah[§]

*Departments of Mechanical Engineering and Chemistry, University of Minnesota and the Minnesota Supercomputer Institute, Minneapolis, Minnesota 55455*

The properties of silica clusters at temperatures from 1500 to 2800 K are investigated using classical molecular dynamics simulations for particles containing up to 1152 atoms. We found that atoms in the cluster were arranged in a shell-like structure at low temperatures, and that the radial density profile peaked near the outer edge of the particle. Smaller clusters have much higher pressures, with the magnitudes corresponding quite well to those obtained from the Laplace–Young equation, when evaluated in a self-consistent manner using our derived surface tension. Our computed surface tension did not show any significant size-dependent behavior in contrast to the decreasing surface tension observed for Lennard–Jones liquid clusters. Finally our computed diffusion coefficients in the liquid state are seen to be larger than bulk computed diffusivities. A discussion regarding the relevance of these computations on the growth of silica nanoparticles is presented.

## I. INTRODUCTION

One of the most import methods of synthesizing nanoparticles is through vapor phase nucleation and growth. Several methods are used, including combustion, plasmas, thermal reactors, and evaporation-condensation.[1–3] The evolution of an aerosol undergoing a gas-to-particle growth process is described by a master equation, the ''aerosol general dynamic equation'' (GDE).[4] The GDE is a population balance equation for the behavior in time and space of the particle size distribution function, which can include all the driving forces for particle growth (nucleation, surface growth, coagulation/coalescence, transport, etc.). Less conventionally, but of interest for nanoparticle synthesis research, the GDE can be extended to track the degree of coalescence of particle aggregates.[5] One of the biggest challenges in the implementation of the GDE is knowledge of the rates of these individual processes. For nanoparticle synthesis, one of the most fundamental and important kinetic properties of interest in nanoparticle growth is the sintering or coalescence rate between particles during vapor-phase growth. A knowledge of these rates and their dependence on process parameters ultimately impacts the ability to control primary particle and agglomerate growth, which are of critical importance to nanoscale particles whose properties depend strongly on size, morphology, and crystal structure.[6]

Previous experimental and theoretical studies of sintering in flame reactors demonstrated good agreement for the case of titania particle growth,[7–9] based on a characteristic coalescence time obtained from a solid-state diffusion model, in which the characteristic time is written as

$$\tau_f = 3 k_B T v_p / 64 \pi D \sigma v_0, \qquad (1)$$

where $T$ is the gas temperature, $v_p$ is the particle volume, $D$ is the diffusion coefficient usually reported as an Arrhenious function of the temperature,[10] $\sigma$ is the surface tension, and $v_0$ is the molecular volume for diffusion. In the case of silicon dioxide (silica), however, the primary particle size is typically underpredicted based on a viscous flow coalescence time written as

$$\tau_f = 2 \eta R_p / \sigma, \qquad (2)$$

where $\eta$ is the viscosity,[11] and $R_p$ is the radius of the particle. Ehrman *et al.*[7] discussed the possible causes of the enhanced rate of silica particle sintering observed in an experiment, including the presence of impurities such as alkali metals which could result in a lower viscosity of silica. On the other hand, in theoretical considerations kinetic coefficients such as the diffusion coefficient and the viscosity, as well as the surface tension, were taken from the properties of bulk material. However, we know that what makes the nanoparticles so interesting is that their fundamental properties are intimately related to the physical size of the component.[6,12] For an example, a 10-nm-diameter iron particle has almost 20% of its atoms on the surface.[13] This high fraction of surface atoms alters properties such as the melting point and presumably the surface tension[14] and accounts for the high reactivity of nanoparticles both toward each other and also toward other materials and gases.

One of the interesting aspects of nanoparticles properties we investigate in this paper is the variation of the internal pressure with particle size, as discussed in Ref. 15. Laplace's equation

$$\Delta P = 2 \sigma / R_p \qquad (3)$$

tells us that the pressure difference between a particle and the surrounding environment $\Delta P$ goes as the surface tension $\sigma$, divided by the particle radius. This implies that as the particle becomes smaller, the pressure will approach infinity as the radius becomes vanishingly small. Of course, this assumes that the surface tension is size independent, but in fact, at some point, the surface tension will tend toward zero. Nevertheless, we should expect that the pressure of a particle can be many hundreds of atmospheres, and may impact the chemical, phase and crystalline structure of particles. For an example, the pressure inside a 10-nm-diameter $TiO_2$ particle [$\sigma = 0.5$ J/m² (Ref. 16)] is on the order of 2000 atmospheres. Such elevated pressures may have a significant impact on properties such as diffusion coefficients[17] and the viscosity, which in turn affect the rates of particle

sintering.[10,11] Given these constraints, data obtained at large grain sizes when extrapolated to smaller dimensions may lead to considerable errors. Experimental studies are certainly desirable for investigating these characteristics; however, experiments aimed at determining the fundamental transport and thermodynamic properties of fine aerosols are not easily obtained, because of the ensemble nature of most studies.

In this paper we study the nanoscale silica clusters of different sizes ($N = 72$, 288, 576, and 1152) and at different temperatures (1500–2800 K), using a classical molecular-dynamics (MD) simulation to determine the structural properties, internal pressure, diffusion coefficients, and surface tension. We are particularly interested in the particle size dependence of these properties, and its influence on coalescence/sintering modeling.

## II. MODEL SYSTEM

The clusters consist of $N$ classical atoms which interact through a pair model potential developed by Tsuneyuki *et al.*,[18] which takes into account the steric repulsion due to atomic sizes, screened Coulomb interaction from charge transfer, charge-dipole interactions due to the large electronic polarizability of the anions, and dipole-dipole interactions to mimic the short- and intermediate-order interaction. The interaction potential has an analytical form of the Born-Huggins-Mayer type $V_{ij} = q_i q_j / r_{ij} + a_{ij} \exp(-b_{ij} r_{ij}) - c_{ij}/r_{ij}^6$, where $q_i$ is the charge of the $i$-type atom, $r_{ij}$ is the interatomic distance, and $a_{ij}$, $b_{ij}$, and $c_{ij}$ are the parameters taken from Ref. 18. For higher temperature the potential was modified in Ref. 19 by adding a Lennard-Jones term, in order to avoid the occasional overriding of the O-O repulsion barrier at a shorter interatomic distance at a higher temperature. The modified interatomic interaction is referred to as the TTAMm potential with the form $V_{ij}^* = V_{ij} + 4\epsilon_{ij}[(\sigma_{ij}/r_{ij})^{18} - (\sigma_{ij}/r_{ij})^6]$, where $\epsilon_{ij}$ and $\sigma_{ij}$ are the usual Lennard–Jones parameters specified in.[19]

The equations of motion for each atom was solved using the standard velocity version of the Verlet algorithm.[20,21] In our calculations we constructed a silica cluster with an appropriate number of atoms, and placed it in the center of a spherical cavity of radius $R^*$, which comprised the calculational cell. The center of the calculation cell ($r = 0$) coincides with the center of mass of the cluster. The radius of the cell was kept at 2 nm for all clusters. In order to conserve mass at higher temperatures, we force any cluster fragment which escapes the cluster due to evaporation, and reaches the boundary of the cell, to be elastically reflected. All clusters were initially heated to a high temperature liquid state at $T = 4000$ K. Several clusters were then prepared at a variety of temperatures between 1500 and 2800 K by slow numerical cooling. Clusters were allowed to anneal for 35 000 time steps (with a time step $\delta t = 1$–4 fs), followed by a test at constant energy to evaluate if the system had reached an equilibrium state. Production runs for cluster properties were performed at a fixed temperature, and typically required about $1.5 \times 10^5$ time steps to obtain a reasonable statistical averaging of cluster characteristics. In order to verify the
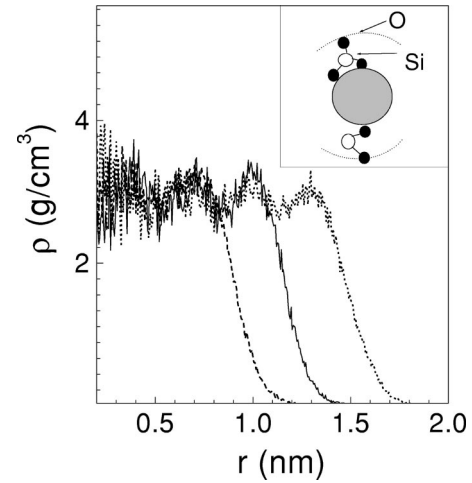


FIG. 1. The radial density distribution for clusters with 288 atoms (dashed line), 576 atoms (solid line) and 1156 atoms (dotted line) at $T = 2080$ K. The sketch of surface structure is shown in the inset.

equilibration procedure for each prepared cluster, we gradually decreased the temperature from 4000 to 1500 K, followed by a reversal of this procedure to the desired target temperature. A comparison of cluster properties such as the radial density distribution, obtained by cooling and then reverse heating, shows good agreement.

The total angular momentum of cluster motion is always reset to zero by the transformation of velocities in order to evaluate transport properties such as diffusion coefficients. We did not analyze the cluster behavior at higher temperatures $T > 3000$ K, where a significant dissociation of fragments takes place during the time interval of the calculation ($t \approx 0.15$ ns). This is because this interatomic potential cannot realistically describe the vaporization processes of silica.[22] For instance, in our calculations we observe the vaporization of $SiO_2$ molecules, while it is well known[23] that silica vaporizes by decomposition to SiO and $O_2$.

## III. RESULTS

### A. Particle density

At lower temperature $T = 1500$ K in a solid "glass" state, all clusters exhibit an oscillating density distribution. With increasing temperature there seems to be a tendency to dampen out the radial density gradient, though some peaks still remain. The radial dependence of the mass densities of different-sized clusters is shown in Fig. 1 at a temperature $T = 2080$ K. Note that the interpeak space is about the mean Si-Si interatom distance which is 0.3175 nm.

To explore the effect of density, in Fig. 2 we show the radial mass density distribution for a 576-atom cluster at three temperatures. It is clear that the radius of the $SiO_2$ nanoparticles and, consequently, the averaged density, are effectively insensitive to temperature over quite a large temperature range (1500–2800 K). This is in accordance with the fact that bulk silica has an extremely low thermal expansion coefficient.[24] Over this temperature interval a cluster
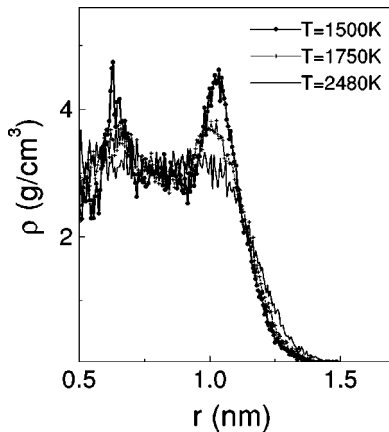
FIG. 2. Radial density distribution for the cluster with 576 atoms at different temperatures.
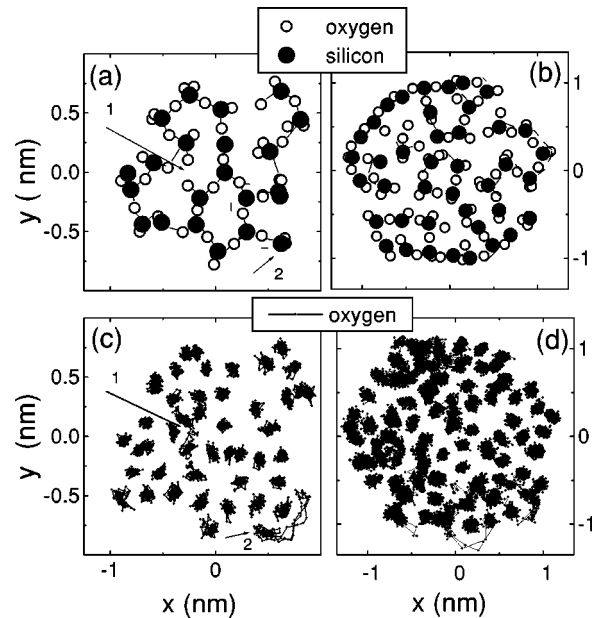


FIG. 3. Averaged oxygen atom positions (open circles) and silicon positions (solid circles) for clusters with 288 atoms (a) and 576 atoms (b). The trajectories of oxygen atoms for the clusters with 288 atoms (c) and 576 atoms (d). Shown is a slice of the clusters at $T = 1500$ K.

with $N = 288$ atoms has a radius $R = 0.92$ nm and an average density of $\rho = 3.2$ g/cm$^3$. The 576-atom cluster has a radius $R = 1.16$ nm and a density $\rho = 2.9$ g/cm$^3$ and the cluster of $N = 1152$ atoms has $R = 1.5$ nm and $\rho = 2.8$ g/cm$^3$. The radius of a cluster is defined as the distance where the density drops to 0.5 of its interior value. Note that smaller clusters have a higher density, but the values are in close agreement with that calculated for bulk silica in the coesite phase, with a density of 2.9 g/cm$^3$.[18,25]

The density profiles presented in Figs. 1 and 2 show that near the surface the clusters have a maximum in the density, just before the rapid decrease at the cluster edge. A similar behavior was observed by Roder *el al.*[26] using a BKS interaction potential.[27] They obtained a density of 2.3 g/cm$^3$. This implies that clusters of different sizes have similar shell structures. Moreover, the cluster surface has the same structure and width regardless of size. The rapid density decrease extends over a distance which is more than a Si-O bond length equal to 0.162 nm. A careful temporal observation makes it clearer that the cluster can be separated into "core" and surface components. On the surface both silicon and oxygen have dangling bonds, with the oxygen atom tending toward the surface (see the inset in Fig. 1). These fragments residing on the surface tend to be highly mobile, so that when averages of the density are taken we see a smooth monotonic decrease in the density profile at the edge of the cluster corresponding to about 0.2–0.3 nm. In general, then, we observe an enhanced density for smaller clusters, small thermal expansion, and an oscillating density profile.

### B. Structure

In order to obtain further insight into this oscillating radial density behavior, we consider the structure of the clusters more closely. Shown in Fig. 3 is a cross-section slice for two different clusters ($N = 288$ and 576 atoms) at $T = 1500$ K. The slice is taken through the center of a cluster of thickness 0.328 nm (which is slightly larger than two of nominal Si-O bond lengths). What is being shown are Si and O atom positions following averaging over 75 ps [Figs. 3(a) and 3(b)] and the trajectories for O atoms recorded every 5 ps [Figs.

3(c) and 3d)]. The slice map of smaller cluster looks like a network of atoms organized in rings [Fig. 3(a)]. The larger cluster has apparently a spherically symmetric shell structure [Fig. 3(b)], and the external shell incorporates both O and Si atoms. The defects in the smaller cluster are denoted by atom trajectories that wander. For an instance, in Figs. 3(a) and 3(c) the arrow labeled by 1 shows a vacancy for a silicon atom. The arrow labeled by 2 is another example of a defect and the enhanced mobility of atoms containing dangling bonds.

The distribution of oxygen and silicon atoms as a function of radial position is presented in Fig. 4 for the cluster prepared with 576 atoms (192 Si atoms and 384 O atoms). It clearly indicates that oxygen is preferentially found on the surface layer of the cluster under all conditions. Note that the change of temperature has a pronounced effect on the internal arrangement of the particles. In particular, at $T = 1600$ K the peak in the Si concentration corresponds to a minimum in the O atom density. With increasing temperature to $T = 1680$ K, we find that a thermally induced structural transition takes place. The second Si peak [labeled by 1 in Figs. 4(a) and 4(b)] shifts, and the second peak in O atoms distribution [labeled by 2 in Fig. 4(a)] disappears and indicates an altogether different shell structure. In order to understand the change in the cluster structure we analyze the angular distribution, varying the temperature. In Fig. 5 the O-Si-O and Si-O-Si angular distributions are shown for a cluster with 576 atoms. At a temperature of $T = 1600$ K, the Si-O-Si angle distribution has two maxima which are at 97.7° and 142°. The former denotes the presence of four member rings, and the latter refers to six member rings. As the temperature increases to $T = 1680$ K, the Si-O-Si angular
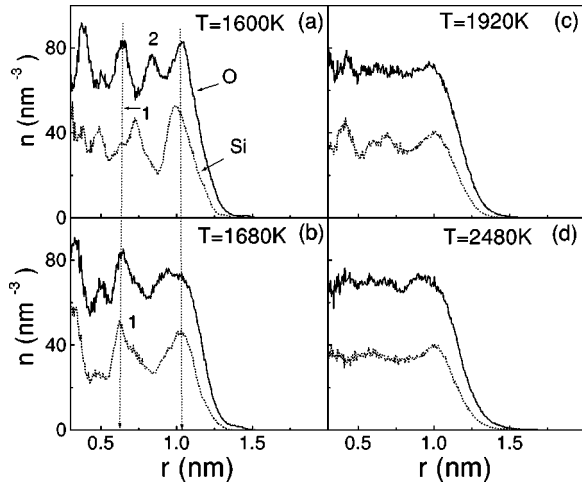
FIG. 4. Averaged radial distribution of oxygen atoms (solid lines) and silicon atoms (dotted lines) in a cluster with 576 atoms at temperatures $T=1600$ K (a), 1680 K (b), 1920 K (c), and 2480 K (d).



FIG. 6. Si-Si pair correlation function for clusters with 288 atoms at $T=1500$ K (solid line), with 576 atoms at $T=1500$ K (triangles) and with 576 atoms at $T=2800$ K (circles).

distribution has only one maximum at 142°. The observation of the angular distribution change clarifies the structural rearrangement in the shell structure presented in Figs. 4(a) and 4(b). Note that the O-Si-O angular distribution only slightly broadens with increasing temperature as expected, and retains a monomodal character. Our results agree well with the angular distributions in the amorphous and molten bulk SiO$_2$ studied by Vashishta et al.[28] who used a three-body potential. For example, at $T=2500$ K the O-Si-O and Si-O-Si angular distributions have maxima at 110.1° and 141° for the cluster with 576 atoms, and at 109.5° and at 142.5°, respectively, for bulk material.[28] The angular distributions are, however, much broader for the clusters compared to the bulk because of the spherical surface and shell structure. A similar broadening was observed by Roder et al.[26]

We calculated the partial pair correlation functions for the O-O, Si-O, and Si-Si bonds to understand the enhanced density of smaller particles and mechanism of cluster expansion at higher temperature. It turns out that the first and second
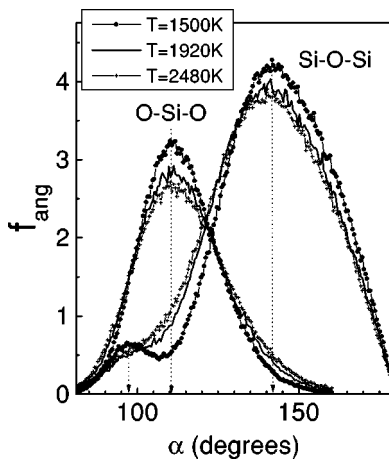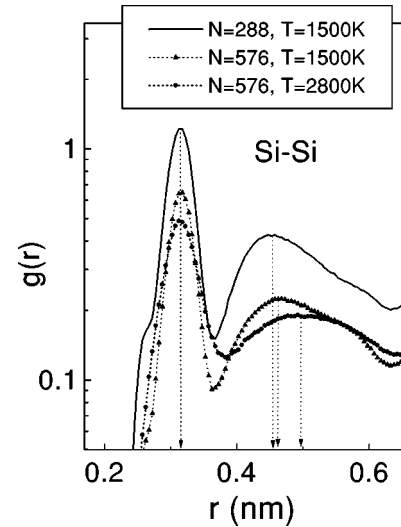
peaks of the O-O and Si-O pair correlation functions have the same positions for all clusters. In contrast to this fact the different clusters have various Si-Si pair correlation functions. One can see in Fig. 6 that the smaller cluster ($N=288$ atoms) has a closer Si-Si packing than the largest one ($N=576$ atoms) at $T=1500$ K.

With increasing temperature the peaks of the O-O and Si-O pair correlation function become broader, and their positions remain independent of temperature, whereas the Si-Si pair correlation function is sensitive to the temperature. Its first peak at $r=0.317$ nm (0.305 nm in Ref. 28) does not respond to temperature, but a second peak shifts to the larger coordinate (see Fig. 6). Thus, we can conclude that the variation of the density with the cluster size as well as the expansion of a cluster with temperature are explained by the change in the Si-Si atom packing due to the strong repulsive nature of the Si-Si interaction.

### C. Melting transition behavior

For a silica cluster as well as for bulk material, the critical temperature of melting can be found by computing the potential energy as a function of temperature. The potential energy per atom $E$ for two clusters with $N=288$ and 576 atoms as a function of temperature is shown in Fig. 7. The potential energy exhibits a change of derivative, denoting the melting within a range of 1670–1800 K for the 288-atom cluster and within 1760–2030 K for the 576-atom cluster, and lower than the melting temperature for the amorphous bulk material (1986 K).

The effect of particle size on the melting point for small clusters has been generically studied. Most recently for example Cleveland et al.[29] studied the melting behavior of small gold clusters. They observed a similar discontinuity in the potential energy, and showed that the melting point was suppressed as the clusters were made smaller. However, in their clusters they observed a very sharp discontinuity and



FIG. 5. Angle distribution for the Si-O-Si and O-Si-O bonds at different temperatures for the 576-atom cluster.
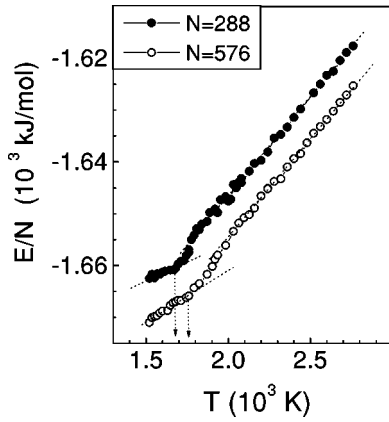
FIG. 7. Potential energy as a function of the temperature for the clusters with $N=288$ atoms (solid circles) and $N=576$ atoms (open circles).

therefore an abrupt melting point. However, our clusters show a much broader transition region, which we believe to be due to the amorphous character of the silica clusters relative to the crystalline gold. We have seen a similar solid-liquid coexistence region in our simulation of the properties of silicon nanoclusters.[14,30] For the cluster sizes studied, the smaller particle had a potential energy per atom that was roughly 7 kJ/mol higher than the larger cluster and was independent of temperature, implying indirectly that the surface energy is size independent. We will consider this point further when we discuss our calculation of the surface tension.

Near the melting temperature we observe that the oxygen radial distribution profile becomes flatter [see Fig. 4(c)], whereas the silicon atoms still show an oscillating density gradient. With a further temperature increase, however, both the Si and O atom distributions become flat. The fact that the density distributions for both elements do not track each other is presumably associated with differences in their ability to move. We calculate the diffusion coefficient of O and Si atoms in a cluster, taking into account the finite size of the system. For an infinite crystal the diffusion coefficient $D$ in the time limit $t \to \infty$ can be defined as

$$D = \sum_{n=1}^{N} \langle R_n^2 \rangle / 6Nt, \qquad (4)$$

where $R_n^2$ is the mean-square displacement of the $n$th atom, and $\langle \rangle$ is an average over time. For a finite system such as a cluster it is necessary to separate the transport into three regime. In Fig. 8 the mean square displacement of atoms with time is shown for the smallest cluster ($N=72$ atoms) and a large one ($N=576$ atoms). The first stage of diffusion (I) is characterized by motion of atoms near their equilibrium sites or "cages" created by neighbor atoms. In the second regime (II) the atoms jump from one site to another, and the mean-square displacement increases linearly with time. In the third stage (III) we observe a saturation in the mean-square displacement of atoms because the characteristic diffusion length is of the order of the cluster size. In Fig. 8 one can see all regimes of diffusion for the smaller cluster with
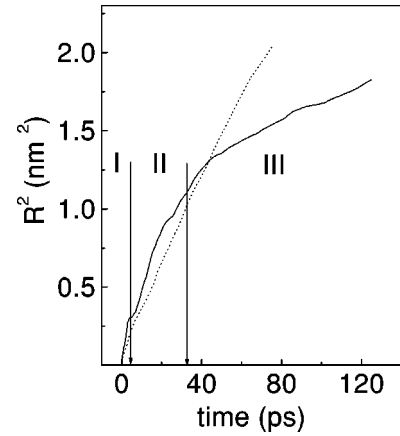


FIG. 8. Mean-square displacements of oxygen atoms in the 72-atom cluster (solid line) and in the 576-atom cluster (dotted line) at $T=2480$ K. Vertical arrays separate different regimes of diffusion (I, II, and III for the 72-atom cluster and I and II for the 576-atom cluster).

72 atoms and only the first two for the 576-atom cluster. The diffusion coefficient for the cluster can be calculated from the second regime through an application of Eq. (4). Note, that for correct calculation of the diffusion coefficient we must exclude the rotation of a cluster as a whole. The computed diffusion coefficients are presented in Fig. 9 for silicon and oxygen atoms in two clusters. The diffusion coefficients are presented in an Arrhenius plot, and give an activation energy $E_A=15\,000$ K for the cluster with 72 atoms and $E_A=16\,100$ K for the cluster with 576 atoms. This is considerably lower that that reported from MD results for bulk silica [$E_A=35\,000$ K (Ref. 31)]. The diffusion coefficient in a small cluster is higher than that for a larger cluster, as one would expect based on surface to volume ratio considerations. Moreover, it has been shown theoretically[32] and experimentally[33] that an increase of the internal pressure (as takes place for smaller clusters and will be discussed below) enhances the diffusion process in silica.

In Fig. 10 we compare the diffusion coefficients for silica obtained from several sources. Our results compare quite well with the MD results from Ref. 28 on bulk silica, although Ref. 28 showed a rather high diffusion coefficient at low temperatures. The cluster results of Roder *et al.*[26]
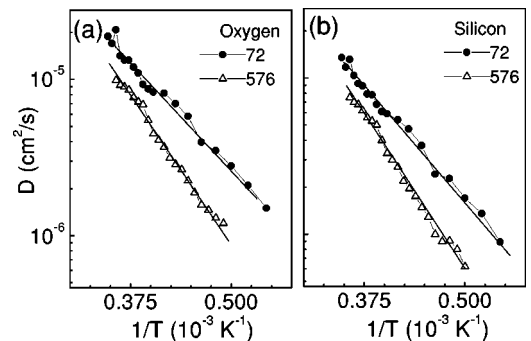


FIG. 9. Diffusion coefficients of oxygen (a) and silicon atoms (b) for clusters with 72 atoms (circles) and 567 atoms (triangles) as a function of inverse temperature.
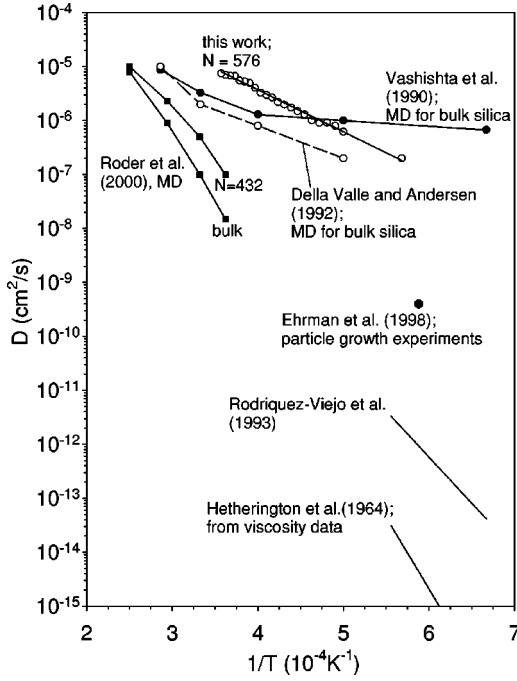
FIG. 10. Diffusion coefficient for silicon atoms from the calculations and experiments.
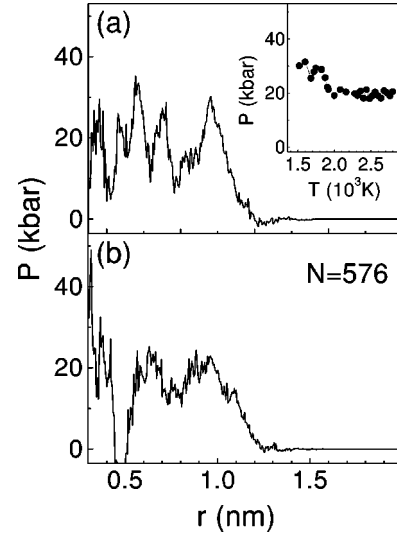


FIG. 11. Radial pressure distribution for the $N=576$ atom cluster at $T=1760$ K (a), and $T=2000$ K (b). Surface pressure as a function of temperature is shown in the inset.

showed a non-Arrhenius behavior, which they attributed to the very high temperature they probed. A comparison of our results to those of Ref. 26 indicates that we obtain significantly higher diffusion coefficients and values that are above bulk, as expected for structures with large surface volume ratio. The diffusion coefficient of silicon atoms is about 30% lower than for oxygen atoms, and agrees with the results for bulk diffusion coefficients.[28]

### D. Internal pressure

The internal pressure of a cluster includes a kinetic part, which is determined by the temperature, and an electrostatic contribution associated with the interactions of the atoms. To obtain the pressure within a particle we compute the Irving-Kirkwood pressure tensor [34] by extension to a spherically symmetric system using the method described by Thompson *et al.*[35] The normal component of the pressure is given as the sum of kinetic and configurational terms $P_N(r)=P_K(r)+P_U(r)$, where the kinetic term is $P_K(r)=k_B T\rho(r)$ and the configurational term is given by

$$P_U(r)=S^{-1}\sum_{k=1} f_k, \qquad (5)$$

where $S=4\pi r^2$ is the area of a spherical surface of radius $r$ and the sum over $k$ is over the normal components $f_k$ of all the pair forces acting across the surface.[35] The normal component of the pressure is calculated by technique described in Ref. 36. We divide our spherical calculation cell into 400 subspheres, which are equidistantly separated by 0.005 nm. We then compute the configurational term of pressure using Eq. (5) for every subsphere surface by computing the normal force component connecting every pair of atoms that reside

across a subsphere boundary. The accuracy of this definition of pressure depends on the number of atoms within the subsphere and therefore quickly diminishes with decreasing radius. The configurational term of pressure $P_U(r)$ is calculated every 500 fs and is averaged over 300 sets.

We found that the internal pressure of clusters lies within a range of (10–30) Kbar, which at 1500 K corresponds to the $\beta$-quartz state on the phase diagram of silica. However, the density of our cluster (2.9–3.2 g/cm$^3$) is considerably higher than the density of $\beta$-quartz (2.5 g/cm$^3$). The radial pressure distribution for the 576-atom cluster shows the sharp peaks in the solid state at $T=1760$ K [Fig. 11(a)] and more smooth profile in the liquid state at $T=2000$ K [Fig. 11(b)]. While the melting transition the surface pressure drops from 30 to 20 kbar (see the inset in Fig. 11).

These sharp peaks actually arises from the oscillating radial density profile (see Figs. 1 and 2) associated with the specific shell structure of clusters. Similar calculations on Lennard-Jones clusters[35] do not show such an oscillatory behavior in either the radial density profile or the internal pressure, because they considered the liquid drops.

In Fig. 12 the smoothed distribution of pressure over radius is shown for three clusters with $N=288$, 576, and 1152 atoms. It is seen that smaller clusters have a higher internal pressure. As was discussed in Sec. I, the internal pressure based on Laplace's equation at constant surface tension predicts a significant increase as a particle shrinks in size, which qualitatively agrees with our MD results.

### E. Surface tension

We calculate the surface tension $\sigma$ within the mechanical approach, following the algorithm described by Thompson *et al.* in Ref. 35. The equation for surface tension for a drop is obtained from Refs. 37, and given by

$$\sigma^3=-\frac{P^2}{8}\int_0^\infty r^3\frac{dP_N(r)}{dr}dr, \qquad (6)$$
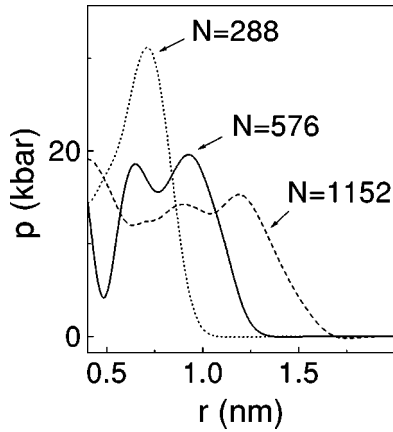
FIG. 12. The smoothed radial pressure distribution for clusters with $N=288$ atoms (dotted line), $N=576$ atoms (solid line) and $N=1152$ atoms (dashed lined line) at $T=2000$ K.

where $P$ is the averaged pressure inside the cluster. The surface tension is obtained by computing the radial distribution of the normal component of the pressure tensor $P_N(r)$ following by evaluation of the integral. One can see from Eq. (6) that the pressure near the surface makes the largest contribution in the surface tension because of the largest pressure gradient. The surface tension as a function of temperature for two clusters is shown in Fig. 13. The most interesting observation is that the surface tension does not depend on the particle size over a large interval of temperature. This is direct contrast to the work of Thompson *et al.*[35] on Lennard-Jones clusters. They observed a significant decrease in surface tension for very small clusters. One possible explanation is that the directional nature of the covalent bonding precludes the surface atoms from adopting configurations that are significantly different; therefore, one should not expect to see surface tensions that are significantly different until one perhaps goes to extremely small clusters. In this case our interaction potential, which is tuned for a bulk-
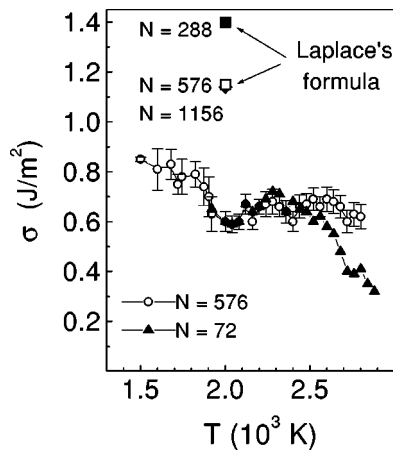


FIG. 13. Surface tension as a function of the temperature for the clusters with $N=72$ atoms (triangulars) and $N=576$ atoms (open circles). The three points above denote the surface tension from Laplace's formula for the clusters with 288 atoms (squares), 576 atom (diamonds), and 1156 atoms (open squares).

like character, will probably fail. This result has significant implications for our interest in sintering behavior, which we will discuss in Sec. IV.

One can see in Fig. 13 that a small cluster with $N=72$ atoms and a larger cluster with $N=576$ atoms have the same value of surface tension at $T=1920$–$2500$ K. At higher temperature the smaller cluster loses its spherical shape, and the probability of dissociation of the $SiO_2$ fragment quickly increases. Therefore, the surface tension of the 72-atom cluster quickly decreases at $T>2500$ K. In our calculations we have obtained a surface tension which is equal to 0.67 J/m$^2$, that is higher than the plane surface tension $\sigma=0.3$ J/m$^2$. We attribute this difference to the interatomic potential chosen for our calculations. The surface tension calculated on the basis of Laplace's formula [Eq. (3)] is essentially larger. For instance, for the $N=288$ atom cluster Laplace's formula overestimates the surface tension by factor of 2.3. The surface tension computed from Laplace's formula for three clusters at the $T=2000$ K is shown in Fig. 13.

## IV. IMPLICATIONS FOR THE COALESCENCE OF SILICA NANOPARTICLES

These studies revealed that surface tension is relatively independent of particle size. Thus we can conclude that the main uncertainty when modeling nanoparticle coalescence, using Eqs. (1) and (2), comes from not knowing the diffusion coefficient and/or the viscosity coefficient as a function on particle size. Experiments (see Ref. 7, for example) allow us to estimate the diffusion coefficient to a reasonable degree, using the method of characteristic times.[38] This method applies especially well to a monotonically cooling system, as is the case in Ref. 7. In such a system, at high temperatures the coalescence time $\tau_f$ is much shorter than the collision time $\tau_c$, i.e., the mean time between collisions. Thus the particles remain spherical. At some point, when the temperature is low enough, $\tau_f$ becomes lower than $\tau_c$, which means that colliding particles do not have enough time to coalesce before a new collision. This is the onset of agglomerate formation, and approximately the point where the primary particle size is determined. The collision time can be estimated from[4]

$$\tau_c = \frac{1}{v_p}\frac{dv_p}{dt} = \frac{\alpha}{2}\left(\frac{6k_BT}{\rho_p}\right)^{1/2}\left(\frac{3}{4\pi}\right)^{1/6}\phi v_p^{-5/6} \qquad (7)$$

in which $\alpha$ is a constant ($\approx 6.67$), $\rho_p$ the particle density, $\phi$ the particle volume loading, and $v_p$ the mean particle volume. For the conditions of Ref. 7, with 10-nm primary particles, the collision time at the onset of agglomerate formation is 0.3 ms. At this point, the coalescence time, given by Eq. (1), should have the same value. This enables us to calculate the diffusion coefficient: $4\times10^{-10}$ cm$^2$/s. The temperature in this system is about 1700 K. One can directly see from Fig. 10 that this value is somewhere between the experimental values for solid bulk silica[39,40] and our MD simulation. At this point it is clear that there is significant discrepancy between the computed growth rate based on our MD calculation and the experiment of Ehrmann *et al.*[7] On the other hand, the derived diffusivity, based on the experimen-

tally determined sintering rate, seems too low, and one has to question whether the temperature ascribed to the growth process is perhaps considerably lower. At this point we are unable to clarify the discrepancy.

## V. CONCLUSION

The structural and dynamical properties of silica nanoclusters were studied in MD simulations with Tsuneyuki *et al.*'s pair potential of interatom interaction. We showed that the clusters have a shell-like internal structure in a solid state, which significantly impacts the radial density profile. Temperature-induced structural transitions in the cluster shell structure at $T = 1680$ K were observed. This rearrangement was associated with change of the Si-O-Si angular distribution from a bimodal shape to a monomodal shape. The melting point phase transition was observed to be suppressed over the bulk value, and a size-dependent melting transition was observed. Cluster expansion and changes in density as a function of temperature were primarily due to changes in Si-Si interactions. We found that smaller clusters have a larger density and a higher internal pressure, which matches the Laplace-Young equation qualitatively and in magnitude. Most interesting was that the surface tension did not show any significant size-dependent effects over a range of cluster sizes of 72–1152 atoms.

With regard to particle formation and growth modeling, the diffusion coefficient plays a critical role in determining the primary particle size. At this time we are unable to rationalize the computed transport properties based on growth rates and the computed transport properties based on MD simulation.

*Permanent address: Institute of Theoretical and Applied Mechanics, Novosibirsk 630090, Russia. Email address: ischweig@site.itam.nsc.ru

†Permanent address: University of Helsinki, Finland.

‡Permanent address: National Institute of Standards and Technology, Gaithersburg, Maryland.

§Electronic mail: mrz@me.umn.edu

[1] M. R. Zachariah, M. Aquino-Class, R. D. Shull, and E. Steel, Nanostruct. Mater. **5**, 383 (1995); M. R. Zachariah and W. Tsang, J. Phys. Chem. **99**, 5308 (1995).

[2] K. L. Steffens, M. R. Zachariah, D. P. DuFaux, and R. L. Axelbaum, Chem. Mater. **8**, 1871 (1996).

[3] U. R. Kortshagen, U. V. Bhandarkar, M. T. Swihart, and S. L. Girshick, Pure Appl. Chem. **71**, 1871 (1999).

[4] *Smoke, Dust, and Haze (Fundamentals of Aerosol Dynamics)*, 2nd ed., edited by S. K. Friedlander (Oxford University Press, New York, 2000).

[5] Y. Xiong and S. E. Pratsinis, J. Aerosol Sci. **24**, 283 (1993).

[6] R. W. Siegel, in *Nanophase Materials: Synthesis, Structure and Properties*, edited by F. E. Fujita, Springer Series in Materials Science Vol. 27 (Springer-Verlag, Berlin, 1994).

[7] S. H. Ehrman, S. K. Friedlander, and M. R. Zachariah, J. Aerosol Sci. **29**, 687 (1998).

[8] R. S. Windeler, K. E. J. Lehtinen, and S. K. Friedlander, Aerosol. Sci. Technol. **27**, 174 (1997); R. S. Windeler, K. E. J. Lehtinen, and S. K. Friedlander, *ibid.* **27**, 191 (1997).

[9] P. Biswas, G. Yang, and M. R. Zachariah, Combust. Sci. Technol. **134**, 183 (1998).

[10] S. K. Friedlander and M. K. Wu, Phys. Rev. B **49**, 3622 (1994).

[11] J. Frenkel, J. Phys. **9**, 385 (1945).

[12] M. C. Roco, R. S. Williams, and P. Alivisatos, *Nanotechnology Research Directions* (Kluwer, Dordrecht, 2000).

[13] N. Ichinose, O. Yoshiharu, and S. Kashu, *Superfine Particle Technology* (Springer-Verlag, New York, 1992).

[14] M. R. Zachariah, M. J. Carrier, and E. Blaisten-Barojas, J. Phys. Chem. **100**, 14 856 (1996).

[15] S. H. Ehrman, J. Colloid Interface Sci. **182**, 606 (1999).

[16] R. H. Bruce, in *Science of Ceramics*, edited by G. H. Steward (Academic, New York, 1965), Vol. 2, p. 359.

[17] B. T. Poe, P. F. McMillan, D. C. Rubie, S. Chakraborty, J. Yarger, and J. Diefenbacher, Science **276**, 1245 (1997).

[18] S. Tsuneyki, M. Tsukuda, H. Aoki, and Y. Matsui, Phys. Rev. Lett. **61**, 869 (1988).

[19] Y. Guissani and B. Guillot, J. Chem. Phys. **104**, 7633 (1996).

[20] L. Verlet, Phys. Rev. **159**, 98 (1967).

[21] M. P. Allen, and D. J. Tildesley, *Computer Simulation of Liquids* (Oxford Science Press, Oxford, 1987).

[22] J. A. Tossel, and D. J. Vaughan, *Theoretical Geochemistry: Applications of Quantum Mechanics in the Earth and Mineral Sciences* (Oxford University Press, New York, 1992), p. 320.

[23] R. T. Porter, W. A. Chupka, and M. G. Ingbram, J. Chem. Phys. **23**, 216 (1955).

[24] O. V. Mazurin, M. V. Streltsina, and T. P. Shvaiko-Shvaikovskaya, *Handbook of Glass Data* (Elsevier, Amsterdam, 1983).

[25] L. L. Liu, W. A. Bassett, and T. Takahashi, J. Geol. Res. **79**, 1160 (1974).

[26] A. Roder, W. Kob, and K. Binder, J. Chem. Phys. **114**, 7602 (2001).

[27] B. W. N. van Beest, G. J. Kramer, and R. A. van Santen, Phys. Rev. Lett. **64**, 1955 (1990).

[28] P. Vashishta, R. K. Kalia, and J. P. Rino, Phys. Rev. B **41**, 12 197 (1990).

[29] C. L. Cleveland, W. D. Luedtke, and U. Landman, Phys. Rev. B **60**, 5065 (1999).

[30] M. R. Zachariah and M. J. Carrier, J. Aerosol Sci. **30**, 1139 (1999).

[31] R. G. D. Valle and H. C. Anderson, J. Chem. Phys. **97**, 2682 (1992).

[32] C. A. Angell, P. A. Cheeseman, and S. Tamaddon, Science **218**, 885 (1982).

[33] N. Shimizu and I. Kushiro, Geochim. Cosmochim. Acta **48**, 1295 (1984).

[34] J. H. Irving and J. G. Kirkwood, J. Chem. Phys. **18**, 817 (1950).

[35] S. M. Thompson, K. E. Gubbins, J. P. R. B. Walton, R. A. R. Chantry, and J. S. Rawlinson, J. Chem. Phys. **81**, 530 (1984).

[36] D. H. Tsai, J. Chem. Phys. **70**, 1375 (1979).

[37] F. P. Buff, J. Chem. Phys. **23**, 419 (1955).

[38] K. E. J. Lehtinen, R. S. Windeler, and S. K. Friedlander, J. Colloid Interface Sci. **182**, 606 (1996).

[39] G. Hetherington, K. H. Jack, and J. C. Kennedy, Phys. Chem. Glasses **5**, 130 (1964).

[40] J. Rodrequez-Viejo, S. F. Clavaguera, M. T. Mora, and C. Monty, Appl. Phys. Lett. **63**, 1906 (1993).